International Journal of Nanomedicine

Dovepress
Taylor & Francis Group

Open Access Full Text Article

ORIGINAL RESEARCH

FOLR1-Targeted Oxygen-Delivering Nanosomes Enhance Chemo-Induced Apoptosis in Hypoxic Cancer

Gahyun Lee[1], Jiwon Kim[1], Jihyuk Yang[1], Yerin Jang[1], Jaehee Jang[1], Masayoshi Tanaka[2], Tagbo HR Niepa[3,4], Hee-Young Lee[5], Jonghoon Choi[1,6,7]

[1]School of Integrative Engineering, Chung-Ang University, Seoul, 06974, Republic of Korea; [2]Department of Chemical Science and Engineering, Tokyo Institute of Technology, Yokohama-shi, Kanagawa, 226-8503, Japan; [3]Department of Chemical Engineering, Carnegie Mellon University, Pittsburgh, PA, 15213, USA; [4]Department of Biomedical Engineering, Carnegie Mellon University, Pittsburgh, PA, 15213, USA; [5]Department of Chemical Engineering, Kumoh National Institute of Technology, Gumi, 39177, Republic of Korea; [6]Feynman Institute of Technology, Nanomedicine Corporation, Seoul, 06974, Republic of Korea; [7]Feynman Institute of Nanomedicine, Nanopeutics Inc, Lewes, DE, 19958, USA

Correspondence: Jonghoon Choi; Hee-Young Lee, Email nanomed@cau.ac.kr; lhysshr@kumoh.ac.kr

Background: The rapid proliferation of tumor cells increases oxygen demand, while the underdeveloped vasculature limits supply, leading to hypoxia in the tumor microenvironment. This hypoxic condition is a hallmark of solid tumors and contributes to tumor progression, immune suppression, metastasis, and resistance to therapy.

Purpose: This study aimed to counteract tumor hypoxia and improve therapeutic outcomes by delivering both oxygen and the chemotherapeutic agent doxorubicin directly to tumors.

Methods: HON_FA@DOX, a folate-functionalized and perfluorohexane-enhanced liposomal nanosome co-loaded with oxygen and doxorubicin, was developed and characterized based on its physical properties. Its tumor-targeting capability, oxygen delivery efficiency, and therapeutic potential were evaluated under in vitro conditions. Cellular experiments were conducted to assess selective binding, hypoxia modulation, cytotoxicity, and the expression of genes related to apoptosis.

Results: HON_FA@DOX exhibited a doxorubicin encapsulation efficiency of 36.6% and an enhanced oxygen loading capacity of 23.2 mg/L. The nanosomes demonstrated selective binding to FOLR1-expressing tumor cells and sustained release of doxorubicin. This dual-delivery system effectively alleviated hypoxia within the tumor microenvironment and reduced the expression of the hypoxia-related gene HIF-1α by 50%. Furthermore, HON_FA@DOX treatment significantly increased the expression of apoptosis-related genes and mitigated chemotherapy resistance, thereby enhancing the overall anticancer efficacy.

Conclusion: We demonstrated that multifunctional nanosomes delivering both oxygen and doxorubicin effectively alleviated tumor hypoxia and reduced chemotherapy resistance, thereby enhancing anticancer efficacy. This approach presents a promising strategy for addressing tumor hypoxia and may be broadly applicable as an adjunct to conventional cancer therapies.

Keywords: liposome, oxygen delivery, drug delivery, hypoxia, HIF, chemoresistance, folate, FOLR1, doxorubicin, chemotherapy

Introduction

Hypoxia in the Tumor Microenvironment

The tumor microenvironment is characterized by increased consumption of nutrients and oxygen due to the abnormal growth and high metabolic rates of tumor cells.[1–3] Although tumor growth promotes angiogenesis, the resulting blood vessels are irregular, structurally abnormal, and functionally incomplete, resulting in uneven blood supply and inadequate delivery of oxygen and nutrients to tumor cells.[4–6] These factors result in hypoxia, with oxygen partial pressures falling below 10 mmHg—a stark contrast to normal tissues, which typically exhibit oxygen levels between 24 and 66 mmHg in approximately 90% of solid cancers.[7–9]

Received: 23 December 2024
Accepted: 3 May 2025
Published: 28 May 2025

Hypoxia plays a critical role in tumor progression and treatment resistance.[10,11] In the tumor microenvironment, hypoxia activates hypoxia-inducible factors (HIFs), oxygen-dependent transcriptional activators that promote the expression of multiple genes.[12,13] Under normoxic conditions, sufficient oxygen levels enable the oxygen-dependent degradation domain (ODD) of HIF-1α to be hydroxylated by prolyl hydroxylases (PHDs), allowing recognition and binding by von Hippel-Lindau proteins (pVHLs).[14,15] This binding facilitates rapid degradation of HIF-1α via the ubiquitin-proteasome pathway, preventing its accumulation and activation.[16–18] In hypoxic conditions, however, low oxygen levels stabilize HIF-1α by inhibiting PHD activity, as oxygen is an essential cofactor for PHD enzymatic reactions. Without sufficient oxygen, PHD cannot hydroxylate HIF-1α, leaving it unbound by pVHL and thus unable to undergo ubiquitination.[19,20] As a result, HIF-1α, which is degraded under normoxic conditions, accumulates in hypoxia and translocates to the nucleus, where it forms a complex with HIF-1β.[21–23] This complex binds to hypoxia-responsive elements (HRE) in gene promoters, activating the transcription of genes involved in angiogenesis, immune suppression, and other processes critical to tumor survival and progression.[24,25]

When the tumor microenvironment is hypoxic and HIF-1α is activated, it fosters an immunosuppressive environment.[26] Hypoxia inhibits the activity of immune cells, such as T cells, NK cells, and macrophages, and activates immune evasion mechanisms by upregulating PD-L1, an immune checkpoint protein.[27–29] In addition, hypoxia increases the expression of vascular endothelial growth factor (VEGF), which promotes the formation of structurally and functionally abnormal neovessels and increases the mobility and invasiveness of tumor cells, thereby promoting metastasis.[4,30] Hypoxic conditions also contribute to chemotherapeutic resistance. Under hypoxia, the expression of multidrug resistance proteins, such as P-glycoprotein (P-gp) is elevated, which actively expels intracellular drugs, reducing their concentration within the cells.[31–33] Moreover, HIF-1α activation downregulates pro-apoptotic proteins such as Bax and upregulates anti-apoptotic proteins such as Bcl-2.[34] Hypoxia also increases extracellular acidity due to an enhanced Warburg effect—a metabolic shift favoring anaerobic glycolysis—that results in ionic trapping of drugs in the extracellular space, further diminishing drug uptake by tumor cells.[4,35] Therefore, overcoming hypoxia is crucial for effective antitumor therapy.

Tumor-Targeting Oxygen Nanosome and Doxorubicin

Doxorubicin hydrochloride (DOX) is a chemotherapeutic agent effective against various cancers, including ovarian, breast, and bladder cancers.[36,37] DOX induces cell death through multiple mechanisms, such as inhibiting topoisomerase II—an enzyme essential for cell proliferation—as well as causing DNA damage and reactive oxygen species (ROS) production.[38,39] However, DOX is associated with several common and serious side effects, including cardiotoxicity, skin rashes, and hair loss.[40–42]

To address the limitations and side effects of chemotherapy, nanocarrier-based drug-delivery systems have attracted significant interest.[43] Among various nanocarriers, liposomes are particularly promising for delivering drugs and other therapeutic molecules.[44] Liposomes are spherical vehicles composed of a phospholipid bilayer encasing an aqueous interior, capable of carrying both hydrophilic and lipophilic drugs, thereby preventing degradation and allowing controlled drug release.[45,46] Their biofilm-like membrane structure makes liposomes safe, biocompatible, and biodegradable.[47] In addition, with a size of 100–200 nm, liposomes benefit from a long circulation time and enhanced permeability and retention (EPR) effect, enabling preferential accumulation in tumor tissues.[48] This targeting reduces systemic drug exposure, thereby mitigating side effects and improving cancer treatment efficacy.[49,50] As such, liposomes are widely used for the delivery of both oxygen and drugs.

Recently, liposomal drug delivery systems for cancer therapy have been actively researched, incorporating pH-responsive liposomes, stimulus-responsive mechanisms, and multifunctional strategies to enhance anticancer drug delivery.[51–54] However, simply encapsulating a drug within a liposome for sustained release does not guarantee precise tumor targeting. Non-specific distribution may lead to unintended effects on normal cells, reducing treatment specificity and increasing systemic toxicity.[55] Additionally, tumor hypoxia plays a significant role in inducing drug resistance. Oxygen deprivation in tumor tissues upregulates hypoxia-inducible factor-1 alpha (HIF-1α), which enhances cellular mechanisms that promote chemoresistance. As a result, even when anticancer drugs reach tumor cells, their therapeutic efficacy may be significantly reduced due to hypoxia-driven resistance mechanisms.[56] To overcome these challenges, ongoing research aims to develop innovative strategies

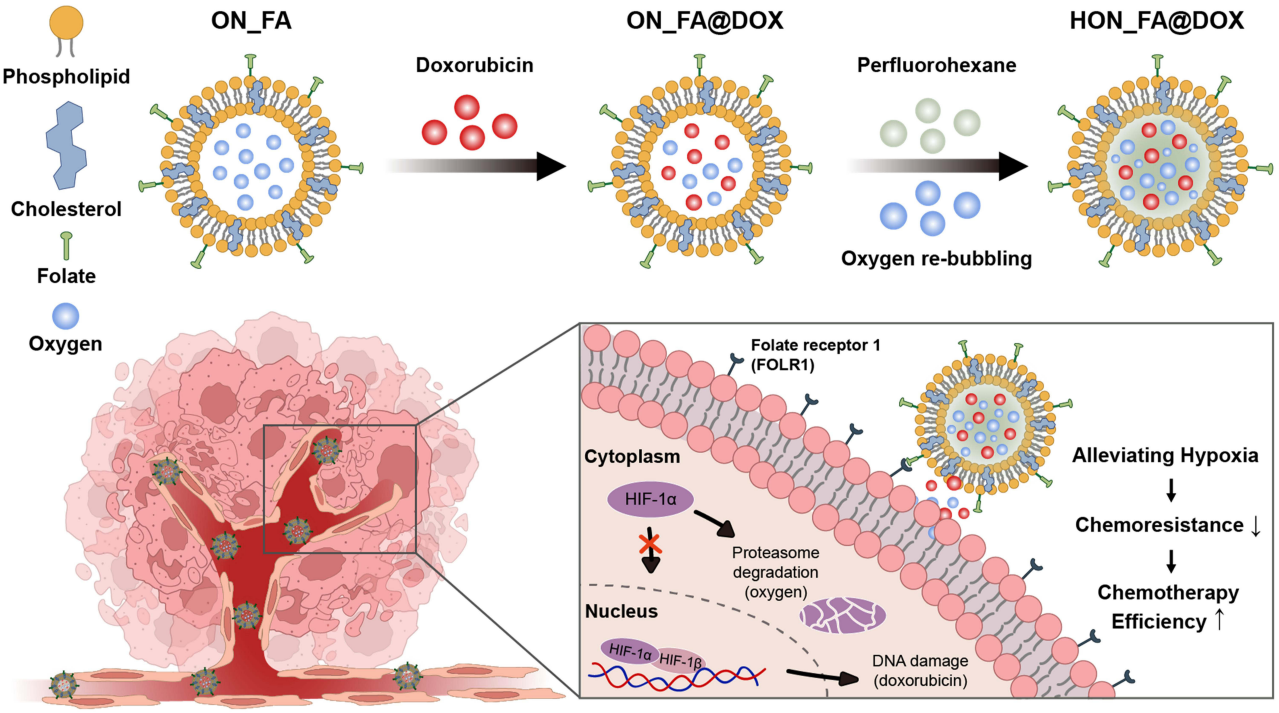

Scheme 1 Schematic of nanosomes designed for specific delivery of oxygen and drugs to tumor microenvironment. Nanosome treatment delivers oxygen and drugs to tumor cells, thereby alleviating hypoxia and reducing chemotherapy resistance.

that address multiple limitations simultaneously. A multifunctional liposomal delivery system capable of precise tumor targeting, oxygen delivery, and chemotherapy is essential to enhance drug efficacy and improve cancer treatment outcomes.[57,58]

Hyperbaric Oxygen Therapy is a common method for oxygen delivery, supplying 100% oxygen at high pressure, but its limitations, including vasoconstriction, cytotoxicity, high costs, and long treatment durations, have driven interest in localized oxygen delivery. While oxygen micro/nanobubbles have been explored, their low stability and risk of gas embolism remain concerns. In contrast, oxygen nanosomes, with their lipid bilayer structure, offer greater stability and functional versatility, allowing for enhanced oxygen delivery and the integration of chemotherapy, immunotherapy, and other cancer treatment strategies.[59,60]

Folate Receptor Alpha (FOLR1) is a membrane protein responsible for folate transport into cells, and it is overexpressed in various cancer types. The upregulation of FOLR1 enhances folate uptake, stimulating the repair of damaged DNA and ultimately promoting tumor growth and metastasis.[61,62] FOLR1 plays a critical role in tumor development and has been identified in cervical and breast cancers, as well as ovarian cancer, non-small cell lung cancer (NSCLC), colorectal cancer, and several other malignancies.[63] Unlike other biomarkers, including EGFR and HER2, which are expressed in normal tissues and may cause systemic toxicity, FOLR1 is predominantly localized on the apical membrane of epithelial cells, minimizing exposure to circulating drugs. Furthermore, its efficient internalization via endocytosis enhances the effectiveness of targeted therapies. Given these advantages, FOLR1 has emerged as a promising target for cancer therapy. Various strategies have been explored, including antibody-drug conjugates (ADCs) targeting FOLR1 and folate receptor-targeted nanoparticles for improved chemotherapy and oxygen delivery.[64]

In this study, we developed nanosized liposomes capable of specifically delivering oxygen and chemotherapeutic agents to tumor cells as a strategy for antitumor therapy and for countering hypoxia (Scheme 1).

https://doi.org/10.2147/IJN.S513688

Materials and Methods

Materials

DSPC (18:0 PC) (1,2-distearoyl-sn-glycero-3-phosphocholine) and 18:0 PEG2000 PE (1,2-distearoyl-sn-glycero-3-phosphoethanolamine-N-[methoxy (polyethylene glycol)-2000] (ammonium salt)) were purchased from Avanti Polar Lipid, Inc. (Alabama, USA). DSPE-PEG5000-Folate (1,2-distearoyl-sn-glycero-3-phosphoethanolamine-N-[folate (polyethylene glycol)-5000]) was purchased from Nanosoft Polymers (Winston-Salem, NC, USA). Pure oxygen gas (99.5%) was acquired from GT Korea (Seoul, Korea), and syringe filters were purchased from Whatman (Maidstone, UK). Amicon filters were purchased from Millipore (Burlington, MA, USA). HeLa and CCD-986Sk cell lines were purchased from the Korea Cell Line Bank (Seoul, Korea), and MDA-MB-231 breast cancer cells were purchased from the American Type Culture Collection. MTT reagent (3-(4,5-dimethylthiazol-2-yl)-2,5-diphenyltetrazolium bromide) was purchased from VWR Life Sciences (Radnor, PA, USA). Doxorubicin hydrochloride, perfluorohexane, cholesterol (sigma grade, 99%), dimethyl sulfoxide (DMSO), Triton X-100, 4% paraformaldehyde (PFA), SpectraPor® 6–8 kDa dialysis bags, BioTracker 520 Green Hypoxia dye, and PD 10 desalting columns were all purchased from Sigma-Aldrich (St. Louis, MO, USA). Cell-mounting medium was purchased from Vector Laboratories (Burlingame, CA, USA). PE anti-FOLR1 antibody was purchased from BioLegend (San Diego, CA, USA). Additional reagents including TRIzol RNA isolation, Fast SYBR Green Master Mix, DAPI (40,6-diamidino-2-phenylindole, dihydrochloride; D1306), Hoechst 33342, Vybrant™ DiO, and Vybrant™ DiD cell-labeling solutions were purchased from Thermo Fisher Scientific Inc. (Waltham, MA, USA). The PrimeScript RT reagent kit was purchased from Takara Bio (Shiga, Japan), and DNA oligonucleotide primers were purchased from Bioneer (Daejeon, Korea). The modular incubator chamber was supplied by Billup Rothenberg (San Diego, CA, USA), and gas for hypoxic cell culture (1 cmol/mol O_2, 4.99 cmol/mol CO_2, and N_2 balance) was purchased from Deokyang Gas Co,. Ltd. (Seoul, Korea).

Synthesis of HON_FA@DOX

HON_FA@DOX was synthesized by combining DSPC, cholesterol, 18:0 PEG2000 PE, and DSPE-PEG5000-Folate in chloroform in a glass vial at a molar ratio of 45:40:14:1. The chloroform solution was dried in a 70 °C oven for 2 h. Once a thin white film had formed, 10 mL of DPBS and 1 mg of doxorubicin hydrochloride were added. The lipid solution was then dispersed for 10 min using a bath sonicator (100 W) above the transition temperature. The solution was subsequently saturated with oxygen gas for 3 min, followed by final dispersion using a tip sonicator (on for 2 s/off for 2 s, 5 min, room temperature, 26% amplitude). Next, 100 μL of perfluorohexane was added, and the solution was treated with a bath sonicator (100 W) for 30 min. After all steps were completed, microparticles and impurities were removed using a 0.2 μm PTFE filter. Centrifugal filtration was then performed according to the manufacturer's instructions to eliminate any unloaded drug. Finally, the resulting solution was treated with oxygen gas for an additional 3 min and stored at 4 °C.

Characterization of HON_FA@DOX

Particle size and surface charge were measured using a Zetasizer Pro (Malvern, UK), while particle concentration was determined with a NanoSight LM10 nanoparticle tracking analyzer (Malvern, UK). All samples were diluted to the appropriate concentration for measurement, and the final particle concentration was calculated to account for the dilution factor. Particle shapes and morphologies were analyzed using a JEM-F200 transmission electron microscope (FE-TEM; JEOL Ltd., Japan). Samples were prepared by placing particles on a CF300-Ni copper grid, staining with 2% uranyl acetate, and drying, with images observed at an accelerating voltage of 80 kV. To confirm the DOX-loading characteristics of HON_FA@DOX, absorption spectra from 300 to 600 nm were analyzed using a microplate reader (BioTek/Agilent, USA). Encapsulation efficiency (EE) was calculated by analyzing free DOX in the solution separated via centrifugal filtration.

$$\mathrm{EE}(\%) = \frac{\text{Total amount of drug} - \text{unloaded drug amount}}{\text{Total amount of drug}} \times 100\%$$

The drug release profiles of HON_FA@DOX and free DOX were evaluated using dialysis bags. Each 1 mL sample was placed into a dialysis membrane bag (molecular weight cut-off 6,000–8,000 Da, Spectrum™ Spectra/Por™ 3 RC Dialysis Membrane Tubing, USA), with 10 mL of DPBS containing 30% ethanol as the external buffer. Samples were incubated on an orbital shaker at 37°C. At regular intervals, 1 mL of the sample was withdrawn, and an equal volume of fresh buffer was added to maintain constant conditions. The collected samples were quantified by absorbance measurements.

The oxygen concentration and release capacity of the synthesized particles were measured using a Portable Dissolved Oxygen Meter (ProSolo, YSI Inc., USA). The oxygen concentration of the particles was estimated by measuring the dissolved oxygen level in the solution immediately after particle synthesis, thereby approximating the dissolved oxygen content within the liposomes. The oxygen release capacity was evaluated in an environment where the dissolved oxygen level in DPBS was reduced to 0.2 mg/L by purging with Ar gas. The particles were introduced into deoxygenated DPBS buffer in a sealed environment, followed by an additional 3-minute Ar gas treatment to remove dissolved oxygen from the particle solution. Dissolved oxygen levels were measured every 30 seconds for 40 minutes, and the data were normalized based on the maximum oxygen concentration observed for each sample.

Cell Culture and Hypoxic Environment

HeLa and MDA-MB-231 cells were cultured in high-glucose Dulbecco's modified Eagle's medium (WELGENE, Korea), while CCD-986Sk cells were cultured in ATCC-modified RPMI 1640 medium (Gibco, Thermo fisher Scientific, USA). All culture media were supplemented with 10% fetal bovine serum (FBS; Gibco) and 1% antibiotics-antimycotics (A/A; Hyclone). Cell were cultured at 37°C, 5%, CO_2, and 90–95% humidity in incubator (Visionbionex, Korea). For hypoxic condition Reverse transcription was ions, cells were incubated at 37 °C in a gas mixture of 1% O_2, 4.99% CO_2, and 94.01% N_2, with 90–95% humidity.

Cell Cytotoxicity Test

An MTT assay was used to determine the cytotoxicity of the particles in Hela (Human cervical cancer), MDA-MB-231 (Triple-negative breast cancer) and CCD-986Sk (Human skin fibroblast). Cells were seeded in 96-well plates at a density of 1×10^4 cells/well and incubated at 37 °C for 24 h. After incubation, wells were washed with DPBS and treated with oxygen nanosomes (ONs), ON_FA, HON_FA@DOX, or free DOX at various concentrations in fresh medium. Following sample treatment and two washes with DPBS, 1 mg/mL MTT solution was added and incubated for 1 h. The MTT solution was then removed, and DMSO was added to dissolve the formazan crystals formed. The formazan concentration was measured at 570 nm using a microplate reader (BioTek/Agilent, USA). Results were compared to the viability of a control group that received no treatment.

Flow Cytometry Measurement for FOLR1 Expression

To verify that FOLR1 was overexpressed on the surface of cancer cells but underexpressed on normal cells, flow cytometry analysis was conducted using a FACS Aria II (BD Biosciences, CA, USA). HeLa, MDA-MB-231, and CCD-986Sk cells were seeded in 6-well plates at a concentration of 1×10^6 cells/well and incubated for 24 h. For FACS measurement, cells were gently detached using TryPLE™ Express Enzyme (Gibco), resuspended at 1×10^6 cells/100 μL in 1×PBS with 5% FBS, then incubated with 5 μL of Phycoerythrin (PE) anti-FOLR1 antibody for 1 h at 4 °C in the dark. After incubation, cells were centrifuged at 1000 rpm for 4 min to remove unbound antibodies, then resuspended in 1×PBS containing 5% FBS for flow cytometry. Samples were analyzed using 488 and 633 nm lasers, and data were processed with FlowJo™ v10.8.0 software (BD Life Sciences, Franklin Lakes, NJ, USA).

Cell-Binding Ability Through Folate

Having confirmed that FOLR1 was predominantly overexpressed on cancer cells and minimally expressed on normal cells, we performed binding capacity assays with nanosomes in the presence and absence of folate. HeLa, MDA-MB-231, and CCD-986Sk (control) cells were seeded in 96-well plates at a concentration of 1×10^4 cells/well and incubated for 24 hours. For fluorescence labeling, the phospholipid bilayer of 2 mL of ON and ON_FA particles was incubated with 10 μL of DiO solution for 30 min to label the particles fluorescently, after which free DiO was separated from the particles using

 https://doi.org/10.2147/IJN.S513688

a Sephadex G-25 column. The DiO-labeled ON and ON_FA particles were then added to each well at a lipid concentration of 352 μg/mL and allowed to bind for 3 h at room temperature. After the incubation period, each well was washed twice with 1×PBS to remove unbound particles. The fluorescence of cell-bound particles was measured at λ_{Em} 490 nm and λ_{Ex} 520 nm using a microplate reader (BioTek/Agilent, USA). For further analysis, HeLa, MDA-MB-231, and CCD-986Sk (control) cells were seeded in 12-well plates at a density of 1×10^5 cells/well and cultured for 24 h. After washing with 1×PBS, 5 μL of DiD solution per 1 mL of medium was added to stain the cell membranes, and cells were incubated at 37 °C for 1 h. Cells were then washed with 1×PBS, followed by treatment with DiO-labeled ON and ON_FA particles at the same particle concentration, and incubated at 37 °C for 3 h. After incubation, cells were washed with 1×PBS to remove unbound particles, and coverslips with attached cells were fixed with 2% PFA. Fluorescence images were acquired using a STELLARIS 5 confocal microscope to determine the extent of particle binding.

Hypoxia Staining

HeLa cells were seeded at a density of 1×10^5 cells/2 mL in 12-well plates and incubated under both normoxic and hypoxic conditions for 48 h. After incubation, cells were treated with 5 μM BioTracker hypoxia dye solution, alongside untreated controls and samples of ON_FA and HON_FA@DOX at a concentration of 352 μg/mL (based on lipid concentration). Each cell line was incubated for 1 h under normoxic or hypoxic conditions. The cell culture medium was then removed, cells were washed twice with 1×PBS, and fresh medium was added, followed by an additional 3 h incubation under the respective conditions. Coverslips with attached cells were subsequently washed twice with 1×PBS, fixed with 2% PFA, and mounted on glass slides. Hypoxic dye fluorescence was visualized using a STELLARIS 5 confocal microscope (LEICA).

Confirmation of HIF-1α and Apoptosis Gene by RT-qPCR

RT-qPCR analysis was conducted to confirm hypoxia relief and tumor cell death induced by the particles. Hypoxia relief was evaluated by analyzing the expression level of HIF-1α using RT-qPCR, while tumor cell death was assessed by analyzing the expression levels of P53, Caspase-3, and BAX. Detailed information about the primers is provided in Table S1. For RNA extraction, HeLa cells were seeded into 6-well plates at a concentration of 3×10^5 cells/well and incubated under normoxic and hypoxic conditions at 37 °C for 48 h. Samples were treated with particles at a concentration of 352 μg/mL (based on lipid concentration) and incubated under the respective oxygen conditions for 4 h. Each well was washed with DPBS, and cells were harvested using TRIzol reagent for RNA extraction. The concentration and purity of the extracted RNA were determined by measuring absorbance at 260 and 280 nm using a microplate reader (BioTek, USA). Reverse transcription was performed using 1000 ng of total RNA with the the PrimeScript™ RT reagent kit (Takara Bio, Japan), and cDNA was synthesized with Bioneer DNA Oligo primers (Bioneer, Korea). The cDNA was diluted 10-fold with DEPC-treated water to prepare samples for RT-qPCR. RT-qPCR was carried out using Fast SYBR Green Master Mix (Applied Biosystems) and the cDNA samples. RT-qPCR analysis was performed on a StepOnePlus Real-Time PCR system (Life Technologies, USA), with the following conditions: initial denaturation at 95°C for 10 min; followed by 40 cycles at 95°C for 15s, 60°C for 1 min, and a final step at 95°C for 15s.

Statistical Analysis

All data and graphs were processed using GraphPad Prism 7.0 for Windows (GraphPad Software Inc., La Jolla, CA, USA). Statistical analysis was performed using one-way ANOVA followed by Tukey's multiple-comparison test in GraphPad Prism 7.0. Each experiment was performed in duplicate, with error bars in the figures representing standard deviations. Significant values are indicated as follows: $*p < 0.1$, $**p < 0.01$, $***p < 0.001$, and $****p < 0.0001$ vs the control, while non-significant values are represented as "ns".

Results and Discussion

Synthesis and Characterization of HON_FA@DOX

In this study, we aimed to target tumor cells specifically and enhance oxygen delivery using ONs, which have previously been employed as oxygen carriers to deliver oxygen and reduce HIF-1 levels.[65–67] To achieve targeted delivery, we incorporated phospholipids containing folate into the nanosome shell. Cholesterol was added to increase the shell's rigidity and stability, resulting in the synthesis of folate-functionalized oxygen nanosomes (ON_FA), an oxygen-delivering liposome. Perfluorohexane (PFH), known for its high gas solubility, was then added to enhance oxygen loading. Additionally, the anticancer drug doxorubicin hydrochloride (DOX) was incorporated, yielding DOX-loaded high-ONs with folate (HON_FA@DOX).[67,68] The synthesized particles were characterized by size, surface charge, particle concentration, and morphology via FE-TEM. Dynamic light scattering measurements showed that the average sizes of ON, ON_FA, and HON_FA@DOX were 117.6 nm, 108.9 nm, and 146.1 nm, respectively indicating an increase in particle size following DOX and PFH loading (Figure 1A, Figure S1). Surface charge analysis revealed that ON, ON_FA, and HON_FA@DOX particles were negatively charged, with average values of −26.36 mV, −17.3 mV, and −10.1 mV, respectively (Figure 1B). Although surface charge increased with DOX and PFH loading, all particles retained a negative charge, suggesting stable dispersion. Nanoparticle tracking analysis showed that the average particle concentrations were approximately 10.42×10^{12} particles/mL for ON, 7.36×10^{12} particles/mL for ON_FA, and 5.10×10^{12} particles/mL for HON_FA@DOX, confirming that sufficient particle quantities were synthesized (Figure 1C). Field emission-transmission electron microscopy (FE-TEM) was used to assess particle morphology. The FE-TEM images confirmed that the particles were spherical phospholipid bilayers, forming liposome-like nanoparticles within the size range of 100–200 nm. These images also indicated that particle morphology was preserved after DOX and PFH loading, consistent with the dynamic light scattering data (Figure 1D). To visually confirm the presence of PFH, images of the sample were taken, showing that PFH was uniformly dispersed, resulting in a cloudy suspension (Figure 1E).

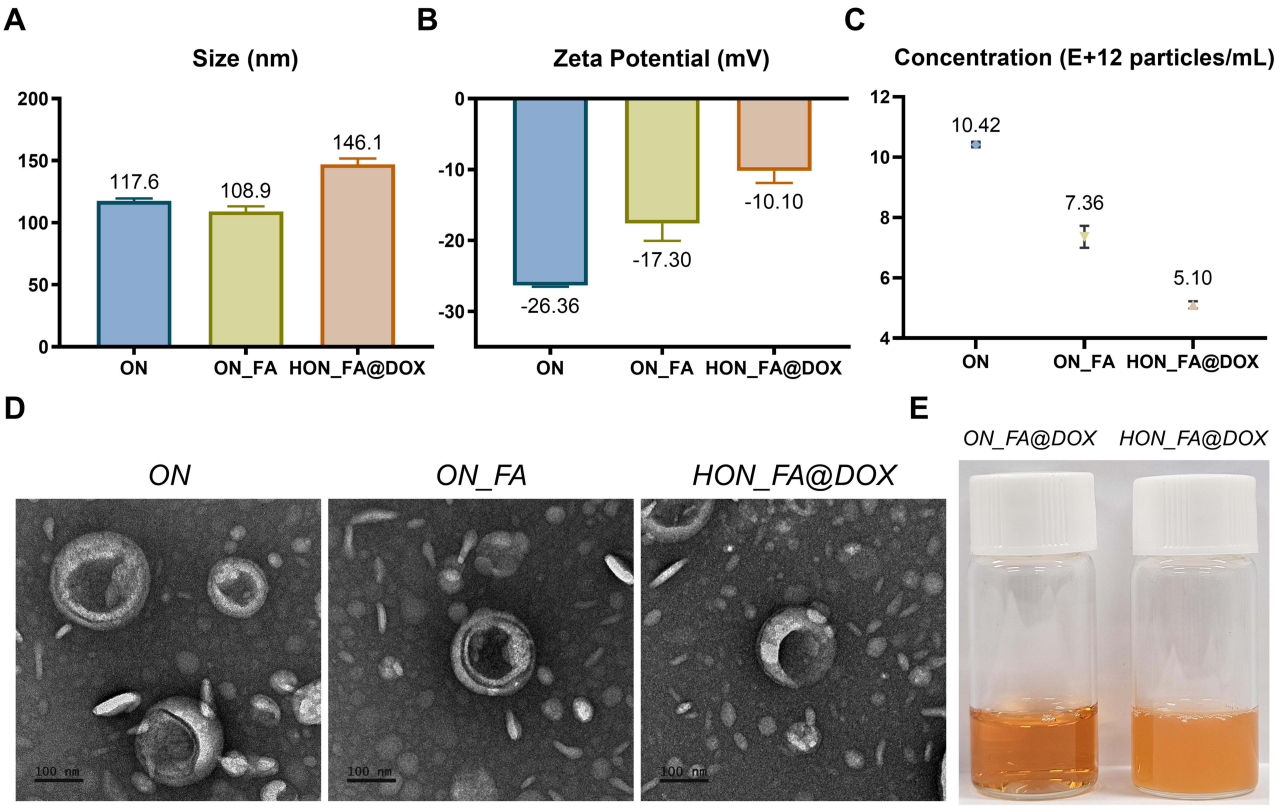

Figure 1 Characterization of ON, ON_FA, and HON_FA@DOX. (**A**) Size. (**B**) Zeta potential of surface particles. (**C**) Particle concentration. (**D**) Transmission electron microscopy images. (**E**) Sample images with and without perfluorohexane.

https://doi.org/10.2147/IJN.S513688

Oxygen and Drug Encapsulation Efficiency and Release

To confirm DOX entrapment within the HON_FA@DOX particles, we compared the absorbance spectra of HON_FA@DOX with those of DOX-free ON_FA particles. Absorbance measurements were conducted over a wavelength range of 300–600 nm. Results showed that HON_FA@DOX successfully encapsulated DOX, as indicated by a prominent absorbance peak at approximately 480 nm—a characteristic feature of DOX—absent in ON_FA (Figure 2A). During HON_FA@DOX synthesis, the DOX feed concentration was 1 mg/10 mL, and the absorbance of the supernatant separated after synthesis was analyzed. A standard curve for DOX was generated, and the EE was calculated to be approximately 36.61% using linear regression (Figure 2B). This encapsulation efficiency, despite the inherent limitations of passive loading, can be attributed to the combined effects of PFH and cholesterol, which enhanced the uniform distribution and stability of DOX·HCl. Cholesterol, in particular, played a crucial role in increasing liposomal stability, reducing DOX leakage, and improving drug retention within the vesicles.[69] To assess drug release behavior, both free DOX and HON_FA@DOX underwent in vitro drug release testing using the dialysis method. For free DOX, 78% of the drug was released within 6 h, with nearly complete release achieved within 12 hours. In contrast, HON_FA@DOX exhibited a slower release profile, with approximately 40% of the drug released after 6 hours, 60% after 12 hours, and 90% after 24 hours (Figure 2C). These findings confirmed the sustained release behavior of HON_FA@DOX, demonstrating controlled release and enhanced DOX delivery via the particles compared to free DOX.

The oxygen concentration of the synthesized particles was measured using an optical dissolved oxygen (DO) meter. In standard DPBS buffer without oxygen-carrying particles, the average oxygen concentration was 8.60 mg/L, whereas it

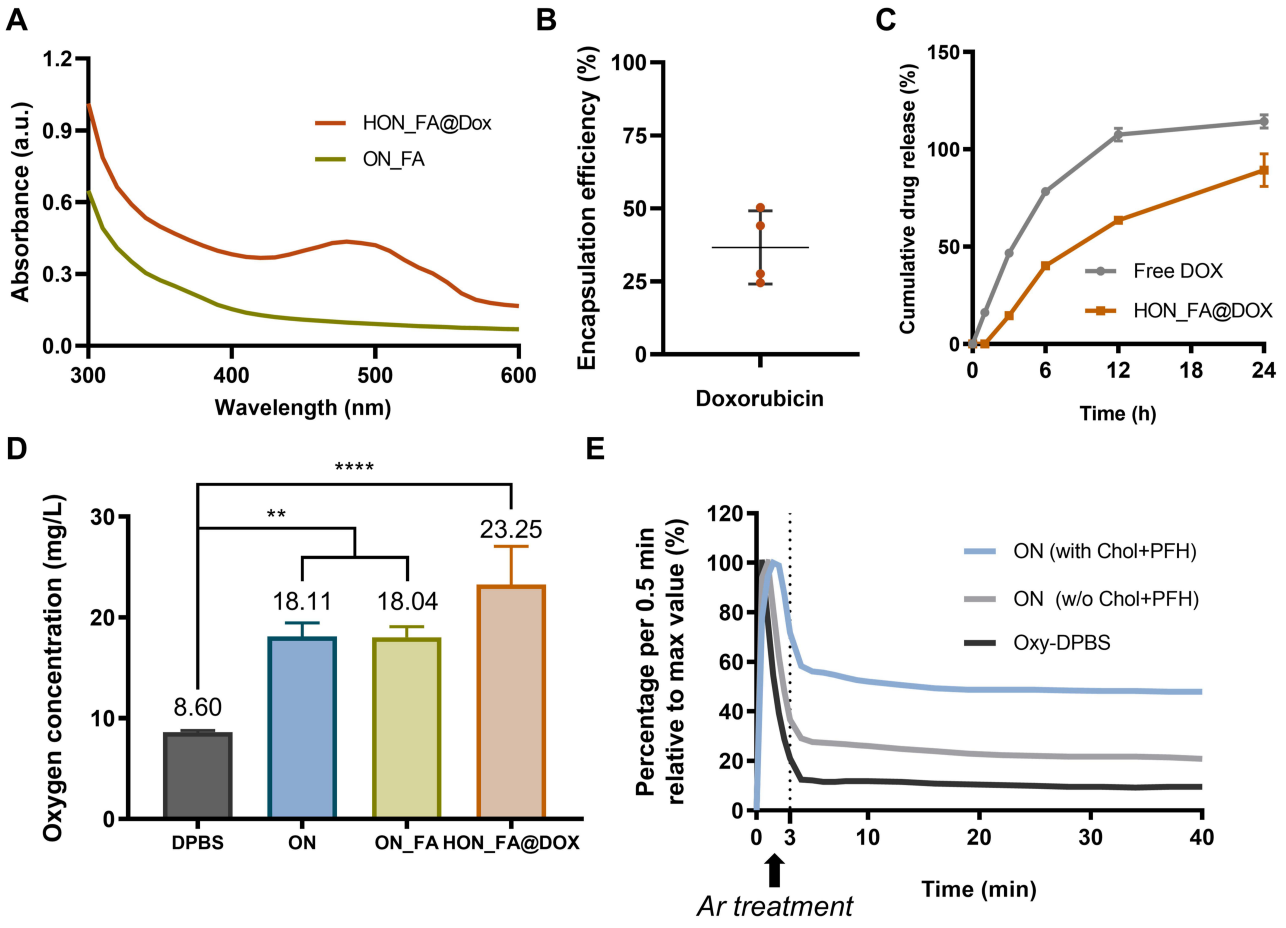

Figure 2 Confirmation of oxygen and drug loading and release. (**A**) Absorbance spectrum. (**B**) Encapsulation efficiency of DOX. (**C**) In vitro cumulative DOX release efficiency from free DOX and HON_FA@DOX at ethanol 30% buffer. (**D**) Oxygen concentration. **p < 0.01, and ****p < 0.0001 compared with the control. (**E**) Normalized oxygen concentration released from oxy-DPBS and oxygen nanosome with and without cholesterol and PFH.

was 18.11 mg/L in ON and 18.04 mg/L in ON_FA, indicating no significant difference in oxygen concentration between particles with and without folate-modified phospholipids. In HON_FA@DOX, the average oxygen concentration increased to 23.25 mg/L, suggesting a higher oxygen content in the particles due to the high gas solubility of PFH (Figure 2D). Next, we assessed the oxygen-release capacity in samples with and without oxygen-carrying particles, as well as with and without PFH and cholesterol. To create a near-anoxic environment, the dissolved oxygen in DPBS buffer was reduced to below 0.2 mg/L by bubbling with argon gas. Oxygen-saturated DPBS (oxy-DPBS), ON without cholesterol or PFH, and ON with cholesterol and PFH were then injected and treated with argon gas for an additional 3 min to deplete dissolved oxygen in the particles. Dissolved oxygen measurements were taken every 30 seconds over a 40-min period, and data were normalized based on the maximum oxygen concentration of each sample. The results showed that oxy-DPBS rapidly lost dissolved oxygen within 5 minutes due to the absence of oxygen transfer particles. However, ON without cholesterol and PFH, and ON with cholesterol and PFH, maintained higher dissolved oxygen levels, attributed to the presence of oxygen transfer particles. Notably, particles containing both cholesterol and PFH exhibited the highest dissolved oxygen levels, attributed to increased shell rigidity and increased oxygen stability (Figure 2E). These findings indicate that the inclusion of cholesterol and PFH contributes to a more stable and effective oxygen transfer in the particles.

Cell Cytotoxicity Test

Since the synthesized particles are designed to deliver both oxygen and DOX to the tumor microenvironment following injection, we evaluated the cytotoxicity of ON, ON_FA, and HON_FA@DOX across varying concentrations to assess the biocompatibility of ON and ON_FA and determine the appropriate treatment concentration for subsequent experiments. ON and ON_FA, which are oxygen-delivering particles without DOX, were found to be biocompatible, showing no toxicity against two cancer cell lines (HeLa and MDA-MB-231) and one normal cell line (CCD-986Sk) (Figure S2). In contrast, the cytotoxicity of HON_FA@DOX was confirmed in the two cancer cell lines due to the presence of the anticancer drug DOX. However, HON_FA@DOX demonstrated relatively milder cytotoxicity compared to free DOX, likely due to the sustained release of the drug as previously observed (Figure 3). However, both HON_FA@DOX and free DOX exhibited cytotoxic effects in both normal and cancer cells, underscoring the need for tumor-specific targeting to ensure safe and effective anticancer drug delivery.

Cell-Binding Ability Through Folate Targeting FOLR1

To validate the tumor-specific targeting capability of ON_FA through folate binding, we first assessed FOLR1 expression in two cancer cell lines (HeLa and MDA-MB-231) and one normal cell line (CCD-986Sk). Typically, FOLR1 is

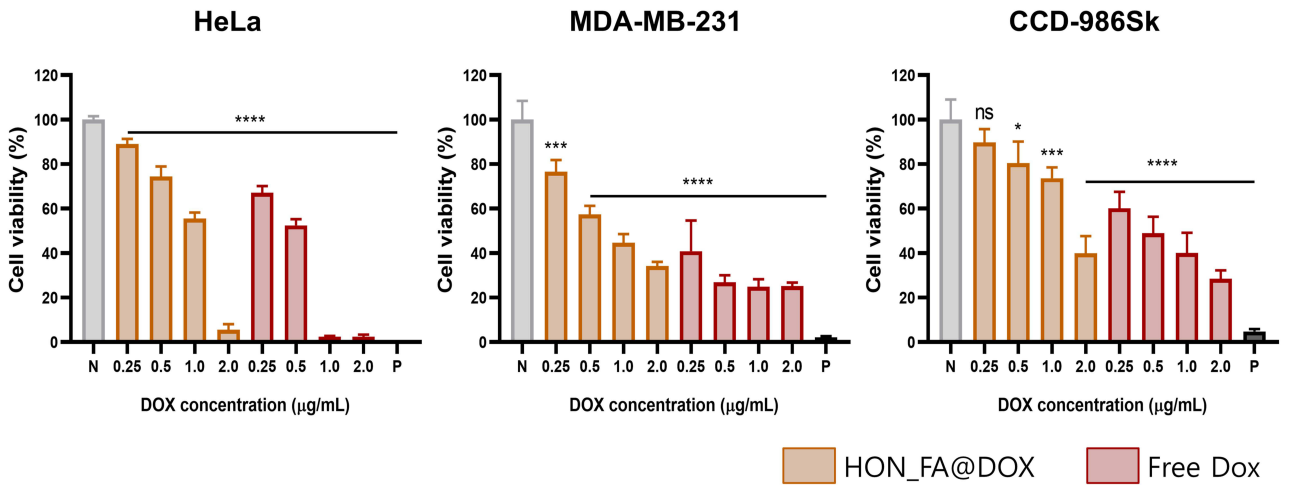

Figure 3 Cytotoxicity test of HON_FA@DOX and free DOX against cancer cells HeLa, MDA-MB-231 and normal cells CCD-986Sk. *p < 0.1, ***p < 0.001, and ****p < 0.0001 compared with the control. "ns" indicates no statistically significant difference.

https://doi.org/10.2147/IJN.S513688

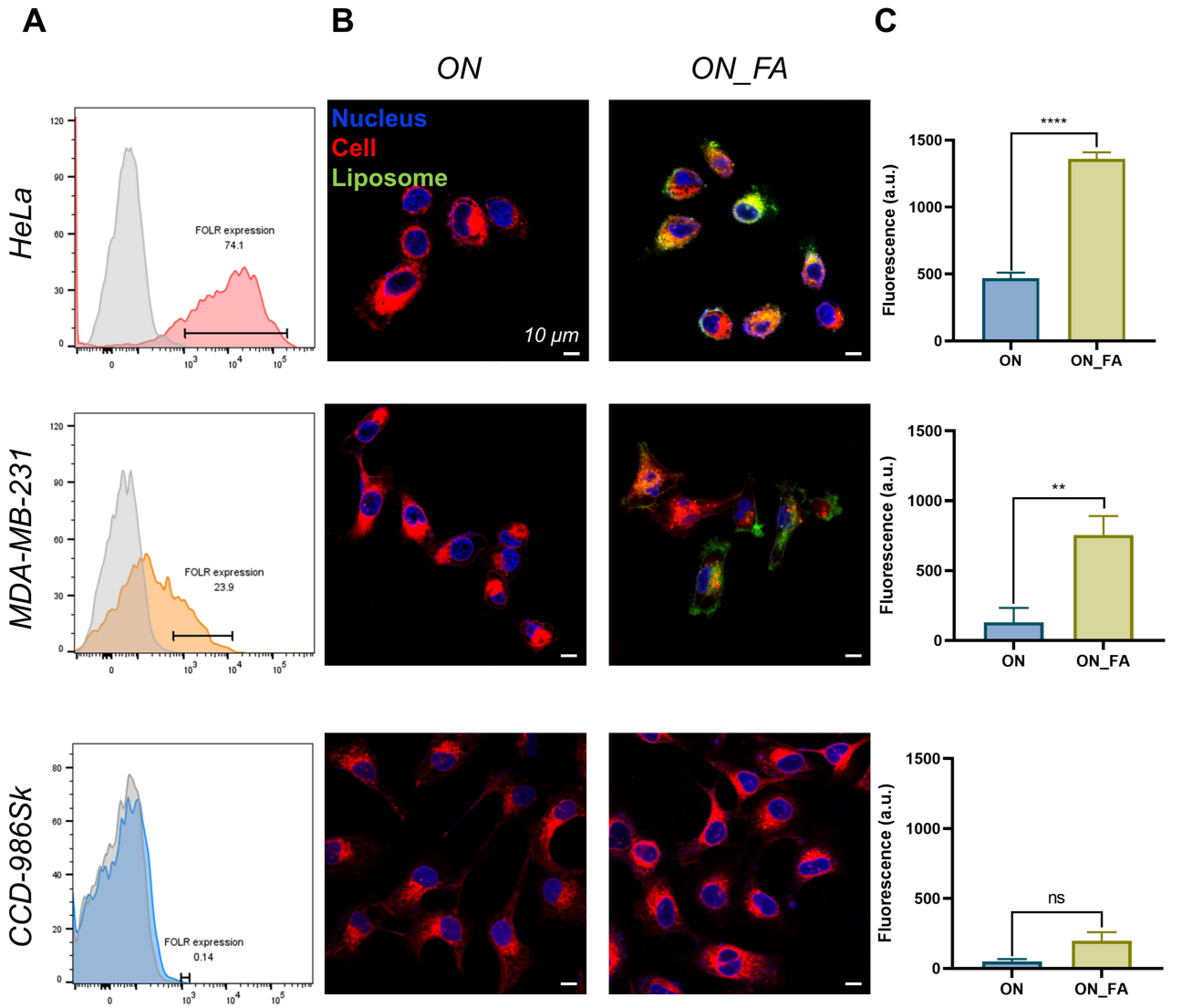

Figure 4 (**A**) FOLR1 expression on cancer cells and normal cells by flow cytometry. (**B**) Comparison of cell-binding ability of ON and ON_FA using confocal images of HeLa, MDA-MB-231, CCD-986Sk cells stained with Hoechst (nucleus, blue), DiD (cell, red), and DiO (liposome, green) (Scale bar = 10 um) (**C**) Quantitative fluorescence analysis of liposomes (green) using a plate reader. **p < 0.01, and ****p < 0.0001 compared with ON. "ns" indicates no statistically significant difference between ON and ON_FA.

overexpressed in epithelial-derived cancers, such as breast and ovarian cancer cells, but not in normal cells. Flow cytometry analysis confirmed this pattern, showing high FOLR1 expression in cancer cells while barely detectable levels were observed in the normal cell line (Figure 4A).

These results indicate that FOLR1-mediated delivery of particles with phospholipids and folate could enable tumor-specific targeting. To verify this, we assessed the cell-binding capacity of ON_FA, a folate-functionalized particle, compared with ON particles lacking folate. Confocal imaging revealed that ON_FA exhibited high green fluorescence on the cell surface and within the cytoplasm of both cancer cell lines, confirming strong FOLR1-mediated binding and rapid intracellular uptake. However, ON particles showed minimal binding to normal cells, with little to no green fluorescence detected on the cell surface or within the cytoplasm (Figure 4B). This difference underscores the selective binding capacity of ON_FA for tumor cells, likely due to efficient folate-mediated binding.

For a quantitative assessment of particle-binding capacity, ON and ON_FA particles were labeled with DiO dye and then applied to two cancer cell lines and one normal cell line, followed by fluorescence measurement using a microplate reader. The results indicated that ON_FA exhibited significantly higher binding capacity to cancer cells, with almost no

binding observed in normal cells, consistent with the confocal imaging results (Figure 4C). These findings confirm that FOLR1 is overexpressed exclusively in cancer cells, allowing folate-functionalized particles to specifically target cancer cells. This specificity suggests that ON_FA could reduce the systemic toxic side effects of DOX while efficiently delivering oxygen to the tumor microenvironment.

Alleviation of Hypoxia

To assess the mitigation of hypoxia through oxygen-delivering particle treatment, HeLa cells—selected for their high binding affinity to ON_FA—were treated with a hypoxia dye, and confocal images were captured. In hypoxic conditions, hypoxia dyes fluoresce green upon reduction, with fluorescence intensity increasing as oxygen levels decrease. Tumor cells were incubated under hypoxic conditions using a gas mixture of 1% oxygen and 5% carbon dioxide. Cells grown under normoxic conditions displayed minimal hypoxia dye fluorescence, while those cultured in hypoxic conditions showed very high green fluorescence, confirming successful hypoxia induction with the gas mixture. Confocal microscopy was then used to determine whether oxygen delivery via ON_FA and HON_FA@DOX could alleviate this hypoxia. Results showed that both ON_FA and HON_FA@DOX treatments significantly reduced green fluorescence intensity compared to untreated cells, indicating effective oxygen delivery by the particles (Figure 5A).

To quantitatively confirm the hypoxia-alleviating effect observed in confocal images, we measured the expression of HIF-1α—a gene typically upregulated under hypoxic conditions—using RT-qPCR. Cells were cultured under both normoxic and hypoxic conditions and treated with either ON_FA, HON_FA@DOX, or left untreated as a control. RNA was extracted, converted to cDNA, and analyzed. The expression levels of HIF-1α mRNA were normalized using the Hypoxia group as the control, with the gene expression level of the Hypoxia group set to 1 (Figure 5B). HIF-1α expression in normoxic cells was approximately half of that in hypoxic cells. In hypoxic cells treated with ON_FA and HON_FA@DOX, HIF-1α expression was reduced by about 30% and 50%, respectively, compared to untreated hypoxic cells. Notably, HON_FA@DOX, enhanced with PFH for higher oxygen-carrying capacity, showed HIF-1α expression levels close to those observed in normoxic conditions (Figure 5B). These findings confirm that the particles developed in this study can effectively alleviate hypoxia in tumor cells.

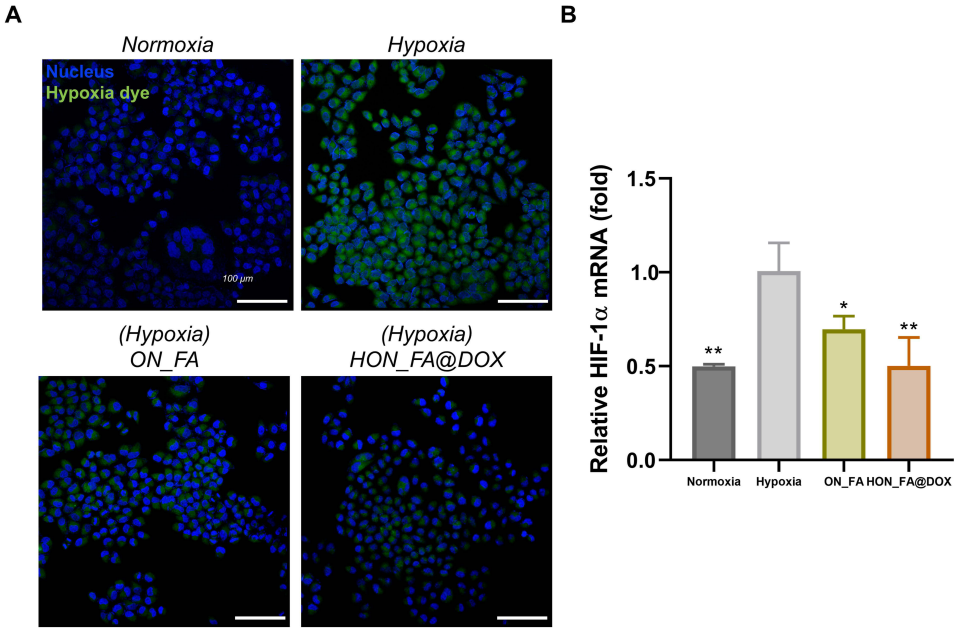

Figure 5 Confirmation of alleviating hypoxia in HeLa cells. (**A**) Changes in hypoxia level as observed by hypoxia dye following ON_FA and HON_FA@DOX treatment. (**B**) Reduction of hypoxia-related gene HIF-1α by particle treatment confirmed through RT-qPCR. *p < 0.1, and **p < 0.01 compared with the control.

https://doi.org/10.2147/IJN.S513688

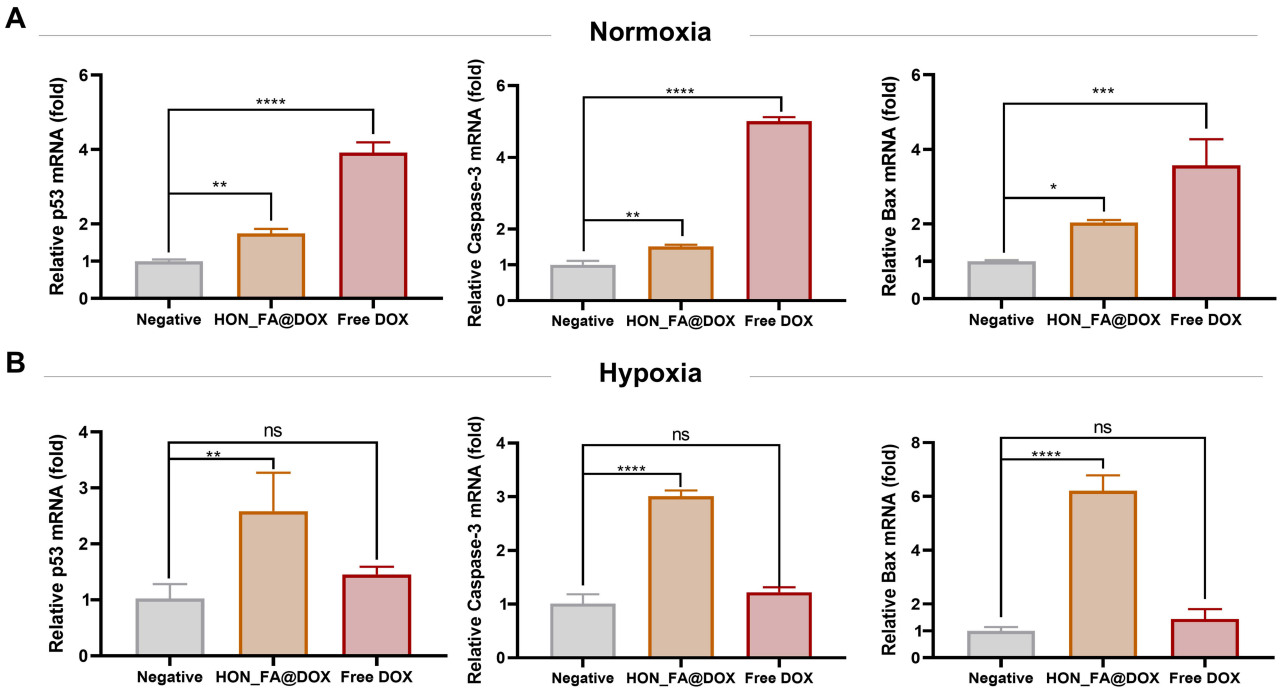

Figure 6 Assessment of HeLa cell apoptosis induction by doxorubicin through RT-qPCR. (**A**) Comparison of apoptosis gene expression in normoxia and (**B**) hypoxia. *p < 0.1, **p < 0.01, ***p < 0.001, and ****p < 0.0001 compared with the control. "ns" indicates no statistically significant difference.

Doxorubicin-Induced Apoptosis in Normoxia and Hypoxia

To determine the apoptotic effects of DOX and alleviating chemotherapy resistance through hypoxia relief, cells cultured under normoxic and hypoxic conditions were treated with HON_FA@DOX and free DOX. RNA was extracted, converted to cDNA, and analyzed by RT-qPCR. p53, a crucial tumor suppressor protein, promotes tumor cell death by upregulating pro-apoptotic proteins essential for apoptosis.[70] Caspase-3 is a primary apoptosis effector, whose activation is irreversible and leads to cell death.[71] Bax, another pro-apoptotic protein, facilitates cell death.[72] Therefore, increased expression of apoptosis-related markers p53, Caspase-3, and Bax was used to confirm tumor cell apoptosis.

In cells cultured under normoxic conditions, HON_FA@DOX and free DOX treatments resulted in increased expression of p53, Bax, and Caspase-3 compared to the untreated control (Figure 6A). However, expression of these apoptosis-related genes was lower in the HON_FA@DOX group compared to free DOX, likely due to the sustained release of DOX. In contrast, under hypoxic conditions, the HON_FA@DOX treatment group exhibited a significant increase in p53, Bax, and Caspase-3 expression compared to the untreated control, while the free DOX group did not show a significant increase in these genes (Figure 6B and C). This lack of response in the free DOX group may be attributed to hypoxia-induced chemotherapy resistance, potentially due to mechanisms like drug efflux or reduced drug uptake. These results suggest that this oxygen-delivering strategy may be more effective at inducing apoptosis in hypoxic tumor cells, making it a promising adjuvant approach to enhance chemotherapy efficiency.

Conclusion

In conclusion, we employed cholesterol and PFH in nanosomes to achieve stable and high-oxygen delivery, incorporated folate to target FOLR1, which is overexpressed in tumor cells, for tumor-specific binding, and loaded the nanosomes with DOX, an anticancer drug, for effective tumor treatment. Characterization of the developed particles confirmed their successful synthesis, cytotoxicity, and tumor cell-specific binding abilities. Furthermore, RT-qPCR and hypoxia staining verified that hypoxia in tumor cells was alleviated by particle treatment. This hypoxia alleviation reduced chemotherapy resistance compared to free DOX, suggesting that DOX-induced cell death was more effectively achieved, as confirmed by RT-qPCR results.

This study demonstrates that FOLR1-targeted oxygen- and drug-delivery nanoparticles offer a novel approach by simultaneously addressing multiple limitations of conventional drug delivery nanoparticles through multifunctionality. By incorporating targeting, drug delivery, and oxygen transport into a single system, we systematically evaluated the individual effects of each function and further confirmed their synergistic impact. Specifically, the oxygen delivery capability effectively alleviated hypoxia, thereby enhancing the therapeutic efficacy of the anticancer drug. This approach represents an innovative, multifunctional strategy for efficient chemotherapy, validating the potential of these nanosomes as a creative and effective drug delivery system. Furthermore, since the developed nanosomes utilize folate-mediated cancer cell targeting, they hold promise as a universal drug carrier applicable not only to cervical and breast cancers but also to other cancer types, including lung cancer.

The in vitro hypoxia model used in this study was designed to provide a precisely controlled oxygen environment, enabling a systematic analysis of the hypoxia-alleviating effects of nanoparticles and their potential to overcome chemotherapy resistance. However, in vitro models alone cannot fully replicate the physiological complexity of the tumor microenvironment. Therefore, future studies should incorporate in vivo models to evaluate the biodistribution, therapeutic efficacy, and long-term safety of the nanoparticles. This approach will allow for a more comprehensive assessment of the clinical applicability of the proposed strategy.

Funding

This research was supported by the Basic Science Research Program through the National Research Foundation of Korea (NRF) funded by the Ministry of Education (No. RS-2023-00275006). This study was also supported by grants from the NRF funded by the Korean Government (MSIT) (No. 2020R1A5A1018052, RS-2024-00469131 and RS-2024-00343605). This work was supported by the Korea Environment Industry & Technology Institute (KEITI) and funded by the Korean Ministry of Environment (MOE) (No. 2022002980003). This research was also supported by the International Collaborative Research and Development Program (P0028061, Development of High-Speed RT-PCR Systems Utilizing Liquid Metal Composites) funded by the Ministry of Trade, Industry & Energy (MOTIE, Republic of Korea).

Disclosure

Dr. Jonghoon Choi is the CEO/Founder of the Feynman Institute of Technology at the Nanomedicine Corp, Seoul, Republic of Korea and the Feynman Institute of Nanomedicine, Nanopeutics Inc., Lewes, DE, United States. The authors report no other conflicts of interest in this work.

References

1. Li Y, Zhao L, Li XF. Hypoxia and the tumor microenvironment. *Technol Cancer Res Treat*. 2021;20:15330338211036304. doi:10.1177/15330338211036304
2. Emami Nejad A, Najafgholian S, Rostami A, et al. The role of hypoxia in the tumor microenvironment and development of cancer stem cell: a novel approach to developing treatment. *Cancer Cell Int*. 2021;21(1):62. doi:10.1186/s12935-020-01719-5
3. Challapalli A, Carroll L, Aboagye EO. Molecular mechanisms of hypoxia in cancer. *Clin Transl Imaging*. 2017;5(3):225–253. doi:10.1007/s40336-017-0231-1
4. Chen Z, Han F, Du Y, et al. Hypoxic microenvironment in cancer: molecular mechanisms and therapeutic interventions. *Signal Transduct Target Ther*. 2023;8(1):70. doi:10.1038/s41392-023-01332-8
5. Chen G, Wu K, Li H, et al. Role of hypoxia in the tumor microenvironment and targeted therapy. *Front Oncol*. 2022;12:961637. doi:10.3389/fonc.2022.961637
6. McKeown SR. Defining normoxia, physoxia and hypoxia in tumours-implications for treatment response. *Br J Radiol*. 2014;87(1035):20130676. doi:10.1259/bjr.20130676
7. Staedtke V, Sun N, Bai R. Hypoxia-targeting bacteria in cancer therapy. *Sem Cancer Biol*. 2024;100:39–48. doi:10.1016/j.semcancer.2024.03.003
8. Vaupel P, Flood AB, Swartz HM. Oxygenation status of malignant tumors vs. normal tissues: critical evaluation and updated data source based on direct measurements with pO2 microsensors. *Appl Magnetic Resonance*. 2021;52(10):1451–1479. doi:10.1007/s00723-021-01383-6
9. Bernauer C, Man YKS, Chisholm JC, et al. Hypoxia and its therapeutic possibilities in paediatric cancers. *Br J Cancer*. 2021;124(3):539–551. doi:10.1038/s41416-020-01107-w
10. Harris B, Saleem S, Cook N, et al. Targeting hypoxia in solid and haematological malignancies. *J Exper Clin Cancer Res*. 2022;41(1). doi:10.1186/s13046-022-02522-y
11. Nam U, Lee S, Ahmad A, et al. Microphysiological systems as organ-specific in vitro vascular models for disease modeling. *BioChip J*. 2024;18(3):345–356. doi:10.1007/s13206-024-00152-4

12. Jaskiewicz M, Moszyńska A, Króliczewski J, et al. The transition from HIF-1 to HIF-2 during prolonged hypoxia results from reactivation of PHDs and HIF1A mRNA instability. *Cell Mol Biol Lett*. 2022;27(1):109. doi:10.1186/s11658-022-00408-7
13. Yfantis A, Mylonis I, Chachami G, et al. Transcriptional response to hypoxia: the role of HIF-1-associated co-regulators. *Cells*. 2023;12(5):798. doi:10.3390/cells12050798
14. Lee J-W, Bae S-H, Jeong J-W, et al. Hypoxia-inducible factor (HIF-1)α: its protein stability and biological functions. *Exp Mol Med*. 2004;36 (1):1–12. doi:10.1038/emm.2004.1
15. Strowitzki MJ, Cummins EP, Taylor CT. Protein hydroxylation by hypoxia-inducible factor (HIF) hydroxylases: unique or ubiquitous? *Cells*. 2019;8(5):384. doi:10.3390/cells8050384
16. Cimmino F, Avitabile M, Lasorsa VA, et al. HIF-1 transcription activity: HIF1A driven response in normoxia and in hypoxia. *BMC Med Genetics*. 2019;20(1):37. doi:10.1186/s12881-019-0767-1
17. Kuschel A, Simon P, Tug S. Functional regulation of HIF-1α under normoxia—is there more than post-translational regulation? *J Cell Physiol*. 2011;227(2):514–524. doi:10.1002/jcp.22798
18. Codony VL, Tavassoli M. Hypoxia-induced therapy resistance: available hypoxia-targeting strategies and current advances in head and neck cancer. *Transl Oncol*. 2021;14(3):101017. doi:10.1016/j.tranon.2021.101017
19. Gonzalez FJ, Xie C, Jiang C. The role of hypoxia-inducible factors in metabolic diseases. *Nat Rev Endocrin*. 2019;15(1):21–32. doi:10.1038/s41574-018-0096-z
20. McAleese CE, Choudhury C, Butcher NJ, et al. Hypoxia-mediated drug resistance in breast cancers. *Cancer Lett*. 2021;502:189–199. doi:10.1016/j.canlet.2020.11.045
21. Taylor CT, Scholz CC. The effect of HIF on metabolism and immunity. *Nat Rev Nephrol*. 2022;18(9):573–587. doi:10.1038/s41581-022-00587-8
22. Eltzschig HK, Bratton DL, Colgan SP. Targeting hypoxia signalling for the treatment of ischaemic and inflammatory diseases. *Nat Rev Drug Discov*. 2014;13(11):852–869. doi:10.1038/nrd4422
23. Giaccia A, Siim BG, Johnson RS. HIF-1 as a target for drug development. *Nat Rev Drug Discov*. 2003;2(10):803–811. doi:10.1038/nrd1199
24. Riemann A, Rauschner M, Gießelmann M, et al. Extracellular acidosis modulates the expression of epithelial-mesenchymal transition (EMT) markers and adhesion of epithelial and tumor cells. *Neoplasia*. 2019;21(5):450–458. doi:10.1016/j.neo.2019.03.004
25. Tirpe AA, Gulei D, Ciortea SM, et al. Hypoxia: overview on hypoxia-mediated mechanisms with a focus on the role of HIF genes. *Int J Mol Sci*. 2019;20(24):6140. doi:10.3390/ijms20246140
26. Rajangam T, Choi JH, Rashid MM, et al. Human dermal fibroblast spheroid overexpressing matrix metalloproteinase-1 serves as a 3D platform for in vitro drug screening. *BioChip J*. 2025:1–16.
27. Wang B, Zhao Q, Zhang Y, et al. Targeting hypoxia in the tumor microenvironment: a potential strategy to improve cancer immunotherapy. *J Exp Clin Cancer Res*. 2021;40(1):24. doi:10.1186/s13046-020-01820-7
28. Fu Z, Mowday AM, Smaill JB, et al. Tumour hypoxia-mediated immunosuppression: mechanisms and therapeutic approaches to improve cancer immunotherapy. *Cells*. 2021;10(5):1006. doi:10.3390/cells10051006
29. Kopecka J, Salaroglio IC, Perez-Ruiz E, et al. Hypoxia as a driver of resistance to immunotherapy. *Drug Resist Updates*. 2021;59:100787. doi:10.1016/j.drup.2021.100787
30. Ramakrishnan S, Anand V, Roy S. Vascular endothelial growth factor signaling in hypoxia and inflammation. *J Neuroimmun Pharmacol*. 2014;9 (2):142–160. doi:10.1007/s11481-014-9531-7
31. Ozcan G. The hypoxia-inducible factor-1alpha in stemness and resistance to chemotherapy in gastric cancer: future directions for therapeutic targeting. *Front Cell Dev Biol*. 2023;11:1082057. doi:10.3389/fcell.2023.1082057
32. Doktorova H, Hrabeta J, Khalil MA, et al. Hypoxia-induced chemoresistance in cancer cells: the role of not only HIF-1. *Biomedical Papers*. 2015;159(2):166–177. doi:10.5507/bp.2015.025
33. Lv Y, Zhao S, Han J, et al. Hypoxia-inducible factor-1α induces multidrug resistance protein in colon cancer. *Oncol Targets Ther*. 2015;8:1941–1948. doi:10.2147/OTT.S82835
34. Jing X, Yang F, Shao C, et al. Role of hypoxia in cancer therapy by regulating the tumor microenvironment. *Mol Cancer*. 2019;18(1):157. doi:10.1186/s12943-019-1089-9
35. Akman M, Belisario DC, Salaroglio IC, et al. Hypoxia, endoplasmic reticulum stress and chemoresistance: dangerous liaisons. *J Exp Clin Cancer Res*. 2021;40(1):28. doi:10.1186/s13046-020-01824-3
36. Park B, Song Y, Youn DH, et al. One-step evaluation of doxorubicin toxicity through concentration gradient generator integrating breast cancer-on-a-chip. *BioChip J*. 2025;1–12.
37. Sung Y, Chang J, Choi S, et al. Synthesis strategies and applications of non-toxic quantum dots. *Korean J Chem Eng*. 2024;41(13):3317–3343. doi:10.1007/s11814-024-00279-y
38. Deng S, Yan T, Jendrny C, et al. Dexrazoxane may prevent doxorubicin-induced DNA damage via depleting both topoisomerase II isoforms. *BMC Cancer*. 2014;14:1–11. doi:10.1186/1471-2407-14-842
39. Lee A, Lee JH, So C, et al. Exosome-immobilized porous microspheres for efficiently combined and prolonged cancer treatment. *Biotechnol and Bioprocess Eng*. 2024;29(5):863–876. doi:10.1007/s12257-024-00139-w
40. Wang S, Konorev EA, Kotamraju S, et al. Doxorubicin induces apoptosis in normal and tumor cells via distinctly different mechanisms: INTERMEDIACY OF H2O2- AND p53-DEPENDENT PATHWAYS*. *J Biol Chem*. 2004;279(24):25535–25543. doi:10.1074/jbc.M400944200
41. Christidi E, Brunham LR. Regulated cell death pathways in doxorubicin-induced cardiotoxicity. *Cell Death Dis*. 2021;12(4):339. doi:10.1038/s41419-021-03614-x
42. Kciuk M, Gielecińska A, Mujwar S, et al. Doxorubicin-an agent with multiple mechanisms of anticancer activity. *Cells*. 2023;12(4):659. doi:10.3390/cells12040659
43. Canlas KKV, Hong J, Chae J, et al. Trends in nano-platforms for the treatment of viral infectious diseases. *Korean J Chem Eng*. 2023;40 (4):706–713. doi:10.1007/s11814-023-1388-0
44. Kim JH, et al. Enhanced drug delivery in cancer therapy: role of TMPRSS4 protease in liposomal engineering. *Biotechnol Bioprocess Eng*. 2025:1–12.
45. Lee G, Choi Y, Hong J, et al. All-rounder liposomes in cancer immunotherapy: strategies and design applications of engineered liposomal nanomaterials. *BioChip J*. 2024;18(2):211–232. doi:10.1007/s13206-024-00147-1

46. Fan Y, Marioli M, Zhang K. Analytical characterization of liposomes and other lipid nanoparticles for drug delivery. *J Pharm Biomed Anal*. 2021;192:113642. doi:10.1016/j.jpba.2020.113642
47. Dymek M, Sikora E. Liposomes as biocompatible and smart delivery systems – the current state. *Adv Colloid Interf Sci*. 2022;309:102757. doi:10.1016/j.cis.2022.102757
48. Ashrafmansouri -S-S, Nasr Esfahany M, Ashrafmansouri -S-S. Mathematical modeling of micro-/nanoparticles transport in blood vessels: a review. *Korean J Chem Eng*. 2024;41(5):1273–1305. doi:10.1007/s11814-024-00071-y
49. Nsairat H, Khater D, Sayed U, et al. Liposomes: structure, composition, types, and clinical applications. *Heliyon*. 2022;8(5):e09394. doi:10.1016/j.heliyon.2022.e09394
50. Tarafdar A, Pula GJ. The role of NADPH oxidases and oxidative stress in neurodegenerative disorders. *Int J Mol Sci*. 2018;19(12):3824. doi:10.3390/ijms19123824
51. AlSawaftah NM, Awad NS, Pitt WG, et al. pH-responsive nanocarriers in cancer therapy. *Polymers*. 2022;14(5):936. doi:10.3390/polym14050936
52. Ashrafizadeh M, Delfi M, Zarrabi A, et al. Stimuli-responsive liposomal nanoformulations in cancer therapy: pre-clinical & clinical approaches. *J Control Release*. 2022;351:50–80. doi:10.1016/j.jconrel.2022.08.001
53. Cheng X, Gao J, Ding Y, et al. Multi-functional liposome: a powerful theranostic nano-platform enhancing photodynamic therapy. *Adv Sci*. 2021;8(16):2100876. doi:10.1002/advs.202100876
54. Zhao F, Wangpimool K, Kim J-C, et al. Near-infrared and Thermo-sensitive liposomes incorporating thiolated-carboxymethyl cellulose-capped gold nanoparticles and poly (N-isopropylacrylamide). *Biotechnol Bioprocess Eng*. 2023;28(4):589–601. doi:10.1007/s12257-022-0378-0
55. Liu Y, Bravo KMC, Liu J. Targeted liposomal drug delivery: a nanoscience and biophysical perspective. *Nanoscale Horizons*. 2021;6(2):78–94. doi:10.1039/D0NH00605J
56. Osada-Oka M, Kuwamura H, Imamiya R, et al. Suppression of the doxorubicin response by hypoxia-inducible factor-1α is strictly dependent on oxygen concentrations under hypoxic conditions. *Eur J Pharmacol*. 2022;920:174845. doi:10.1016/j.ejphar.2022.174845
57. Yang Y, Liu Y, Jiang Y. Recent advances in perfluorocarbon-based delivery systems for cancer theranostics. *Mol Pharm*. 2023;20(7):3254–3277. doi:10.1021/acs.molpharmaceut.3c00116
58. Sheng D, Deng L, Li P, et al. Perfluorocarbon nanodroplets with deep tumor penetration and controlled drug delivery for ultrasound/fluorescence imaging guided breast cancer therapy. *ACS Biomater Sci Eng*. 2021;7(2):605–616. doi:10.1021/acsbiomaterials.0c01333
59. Sayadi LR, Banyard DA, Ziegler ME, et al. Topical oxygen therapy & micro/nanobubbles: a new modality for tissue oxygen delivery. *Int Wound J*. 2018;15(3):363–374. doi:10.1111/iwj.12873
60. Ning S, Zhang X, Suo M, et al. Platelet-derived exosomes hybrid liposomes facilitate uninterrupted singlet oxygen generation to enhance breast cancer immunotherapy. *Cell Rep Phys Sci*. 2023;4(7):101505. doi:10.1016/j.xcrp.2023.101505
61. Yang R, Kolb EA, Qin J, et al. The folate receptor α is frequently overexpressed in osteosarcoma samples and plays a role in the uptake of the physiologic substrate 5-methyltetrahydrofolate. *Clin Cancer Res*. 2007;13(9):2557–2567. doi:10.1158/1078-0432.CCR-06-1343
62. Scaranti M, Cojocaru E, Banerjee S, et al. Exploiting the folate receptor α in oncology. *Nat Rev Clin Oncol*. 2020;17(6):349–359. doi:10.1038/s41571-020-0339-5
63. Varaganti P, Buddolla V, Lakshmi BA, et al. Recent advances in using folate receptor 1 (FOLR1) for cancer diagnosis and treatment, with an emphasis on cancers that affect women. *Life Sci*. 2023;326:121802. doi:10.1016/j.lfs.2023.121802
64. Gonzalez T, Muminovic M, Nano O, et al. Folate receptor alpha—a novel approach to cancer therapy. *Int J Mol Sci*. 2024;25(2):1046. doi:10.3390/ijms25021046
65. Yoon S, Hong J, Park B, et al. Oxygen transport to mammalian cell and bacteria using nano-sized liposomes encapsulating oxygen molecules. *J Biosci Bioeng*. 2021;132(6):657–665. doi:10.1016/j.jbiosc.2021.08.010
66. Hong J, Choi Y, Lee G, et al. Nanosome-mediated delivery of hdac inhibitors and oxygen molecules for the transcriptional reactivation of latent hiv-infected Cd4 + T cells. *Small*. 2023;19(37):2301730. doi:10.1002/smll.202301730
67. Hong J, Yoon S, Choi Y, et al. Rational design of nanoliposomes by tuning their bilayer rigidity for the controlled release of oxygen. *Journal of Molecular Liquids*. 2023;370:121003. doi:10.1016/j.molliq.2022.121003
68. Zeng Q, Qiao L, Cheng L, et al. Perfluorohexane-loaded polymeric nanovesicles with oxygen supply for enhanced sonodynamic therapy. *ACS Biomater Sci Eng*. 2020;6(5):2956–2969. doi:10.1021/acsbiomaterials.0c00407
69. Abraham SA, Waterhouse DN, Mayer LD, et al. The liposomal formulation of doxorubicin. *Methods in Enzymology*. 2005;71–97.
70. Aubrey BJ, Kelly GL, Janic A, et al. How does p53 induce apoptosis and how does this relate to p53-mediated tumour suppression? *Cell Death Differ*. 2018;25(1):104–113. doi:10.1038/cdd.2017.169
71. D'Amelio M, Cavallucci V, Cecconi F. Neuronal caspase-3 signaling: not only cell death. *Cell Death & Differentiation*. 2009;17(7):1104–1114. doi:10.1038/cdd.2009.180
72. Brady HJM, Gil-Gómez G. Molecules in focus Bax. The pro-apoptotic Bcl-2 family member, Bax. *The International Journal of Biochemistry & Cell Biology*. 1998;30(6):647–650. doi:10.1016/S1357-2725(98)00006-5